JOURNAL OF MATERIALS SCIENCE 15 (1980) 1001–1013

Microhardness anisotropy of silicon carbide

G. R. SAWYER,* P. M. SARGENT, T. F. PAGE
Department of Metallurgy and Materials Science, Pembroke Street, Cambridge UK

The effect of crystallographic anisotropy on the room-temperature Knoop microhardness of silicon carbide has been studied on each of three major sections of alpha single crystals (namely: {0 0 0 1}, {1 $\bar{1}$ 0 0} and {1 1 $\bar{2}$ 0}), measurements being made at 10° angular intervals over a range sufficient to include all the non-equivalent indenter orientations on each crystal section. The results are presented graphically and compared with a number of possible anisotropies computed for different slip systems using a model based on the effective resolved shear stress (ERSS) model of Brookes *et al.* [1] with a modification suggested by Arnell [2]. The results are interpreted to show that plastic deformation appears to occur preferentially on the {1 $\bar{1}$ 0 0}⟨1 1 $\bar{2}$ 0⟩ and {0 0 0 1}⟨1 1 $\bar{2}$ 0⟩ slip systems over different ranges of orientations of the indenter. Further, it has been possible to estimate the ratio of the critical resolved shear stresses of these systems, the {0 0 0 1} ⟨1 1 $\bar{2}$ 0⟩ system having a CRSS between 1.2 and 2.1 times that of the {1 $\bar{1}$ 0 0}⟨1 1 $\bar{2}$ 0⟩ system. Computation has also been used to investigate the detailed effect of the form of Brookes' constraint factor and the reliability of hardness anisotropies predicted in this way. The possible roles of slip and other deformation mechanisms in governing the response of brittle solids subjected to indentation hardness tests are also discussed.

1. Introduction

It has been shown by Brookes *et al.* [1] that, using an analysis based on the varying effective resolved shear stress (ERSS) on any member of an operative slip system family, it is possible to explain the observed anisotropy in Knoop microhardness measurements in a range of single-crystal materials in terms of discrete slip-system activity. This potentially simple, non-destructive means of investigating slip behaviour has subsequently been used for correlation with etch pitting and transmission electron microscopy (TEM) dislocation observations (e.g. [1, 3]), for examining the effects of temperature and environment on slip behaviour (e.g. [4, 5]) and, as here, for identifying active slip systems in solids which are brittle in conventional mechanical tests (e.g. transition metal carbides [3–8]). Silicon carbide probably only deforms plastically in response to hardness and wear tests (e.g. [9–12]) and the resultant plastic deformation is highly localized and difficult to study by other techniques (e.g. [12]). However, plasticity is critical in understanding the surface deformation behaviour of such brittle solids in wear- and erosion-resistant engineering applications (e.g. [14]), and this is one objective of the hardness anisotropy study reported here.

Although the analytical model of Brookes *et al.* has proved generally successful, it contains a number of simplifications and assumptions which have been subject to criticism (e.g. [2]) and some of these are discussed in this paper. Some measure of the reliability of the ERSS model has been established from the results of a systematic simulation of the effect of a range of constraint factors (governing the geometry of plastic flow) and an enhanced model has been used to explain the observed room temperature hardness anisotropy of SiC single crystals. Further, it has been possible to derive the ratio of the critical resolved shear

* Present address: The British Rail Research and Development Division, The Railway Technical Centre, London Road, Derby, UK.

0022–2461/80/041001–13$03.30/0

TABLE I Shaffer's hardness data [18]

Plane	Indenter orientation	KHN (100 gf load) (kgf mm^{-2})
$\{0\,0\,0\,1\}$	parallel to $\langle 1\,\bar{1}\,0\,0\rangle$	2954 ± 27
$\{0\,0\,0\,1\}$	parallel to $\langle 1\,\bar{1}\,2\,0\rangle$	2917 ± 10
$\{1\,\bar{1}\,0\,0\}$	parallel to $\langle 0\,0\,0\,1\rangle$	2129 ± 45
$\{1\,\bar{1}\,0\,0\}$	perp. to $\langle 0\,0\,0\,1\rangle$	2755 ± 40
$\{1\,1\,\bar{2}\,0\}$	parallel to $\langle 0\,0\,0\,1\rangle$	2391 ± 34
$\{1\,1\,\bar{2}\,0\}$	perp. to $\langle 0\,0\,0\,1\rangle$	2755 ± 22

stresses (CRSS) of the two slip systems deduced to control hardness anisotropy and to estimate the yield stress of SiC at room temperature.

Some data on the Knoop hardness anisotropy of silicon carbide has been published by Shaffer [15] and this was rationalized in terms of one possible slip system ($\{1\,\bar{1}\,0\,0\}\langle 1\,1\,\bar{2}\,0\rangle$) by Brookes *et al.* [1]. However, these data, which are reproduced in Table I, were limited to two orientations on each of the three principal sections $\{0\,0\,0\,1\}$, $\{1\,\bar{1}\,0\,0\}$, and $\{1\,1\,\bar{2}\,0\}$ and this is insufficient to allow a conclusive identification of the operative slip system to be made. A more comprehensive series of experiments, with data taken at 10° intervals, will be reported here. These measurements reveal detail in the hardness anisotropy not evident in the previous data and allow greater confidence to be placed in the identification of the operative slip systems.

2. Deformation mechanisms – the role of slip

A question central to the ERSS approach concerns the role of slip in determining the hardness response of brittle solids. Firstly it must be appreciated that the stresses generated beneath hardness indenters are complex,* localized, difficult to model, and generally far larger than in any conventional mechanical test. Further, the equilibrium stresses associated with the final *measured* hardness indentation are the *minimum* local stresses experienced as the indenter penetrates the surface. Thus, in hard, stiff solids, *post facto* examination of the indented material may show no evidence of any unusual deformation modes associated with the initial very high stress state, particularly if such processes are either completely reversible (e.g. densification) or leave the material crystallographically perfect (e.g. block shear, which has the same crystallographic character as slip as far as the ERSS model is concerned).

A pressure-sensitive densification mechanism for zinc-blende and wurtzite structure crystals (e.g. SiC) exists, similar to the Tin alpha–beta transition, which has been observed to occur in a large number of IV, IV–IV, III–V, and II–VI elements and compounds using high pressure cells (e.g. [19–21]). Trefilov *et al.* [22] have suggested that the temperature dependence of hardness and microcracking of SiC is similar to that found in Ge, Si and InSb and have tentatively suggested that this is consistent with a metallic transformation occurring.† Further, this densification pressure for SiC has been calculated from thermodynamic data to be 64 GPa [21] which should be compared with 69 GPa (700 kgf mm^{-2}) which is the highest hardness number (H) recorded in the present study for a 50 gf Vickers indentation on SiC $\{0\,0\,0\,1\}$.‡ Block shear may also occur, since Tabor's estimate of the highest shear stress beneath an indenter, of $\sim H/5$ [26], gives a value of 5 to 14 GPa for SiC which compares with a theoretical shear strength ($\sim G/10$) of 19 GPa calculated from available estimates of the moduli [27, 28]. Therefore, it is quite possible that the critical stresses for block shear, and perhaps for densification, will be reached near the tip of the indenter at the beginning of indentation.

* Although the large shear components of this stress state are generally held to be responsible for slip, the hydrostatic component may also affect plasticity in ionic crystals by controlling both the Peierls' stress and dislocation velocity (e.g. [16, 17]). The large tensile stresses produce indentation fracture (e.g. [18]).

† A similar 'crowdionic diffusion' plasticity mechanism has been postulated to occur during indentation of materials of the NaCl structure [23] and has been demonstrated in alumina [24].

‡ SiC displays a pronounced indentation size effect (e.g. [25]) and thus the hardness appears to decrease with increasing load (e.g. 25 GPa for a 500 gf Knoop indentation).

Whatever other deformation mechanism may also occur, slip appears to be an important response of materials to indentation since dislocations have been observed, but not unambiguously characterized by TEM, in association with hardness indentations, wear tracks, and erosive impact sites in silicon carbide [10, 11, 14, 29, 30]. however, etch-pitting of indented SiC single crystals does not produce the rays of pits seen in ionic or metallic crystals (e.g. [31, 32]), the indentation itself being etched away to form a figure which is believed to represent the distribution of residual plastic strain. This technique has been used to identify a possible slip-system controlling indentation on SiC $\{0\,0\,0\,1\}$ as $\{1\,\bar{1}\,0\,l\}\langle 1\,1\,\bar{2}\,0\rangle$ [13]. Dislocations in the proximity of wear tracks in SiC have also been observed to occur at the periphery of a zone of heavily micro-cracked and rotated material which might result from the relaxation of densified material as the local stresses decrease [33]. Thus the role of slip may sometimes be a secondary one in accommodating the displacements from other deformation mechanisms. Further, the fact that, for either predominantly ductile or brittle materials, the trends in hardness *anisotropy* are not dramatically sensitive to variations in load [10, 11, 34], further suggests that slip is the common controlling feature (and sections 4, 5 and 7 treat the phenomenon in this way) but perhaps it does not control the actual equilibrium *hardness pressure* at a given load. This pressure, however, can be thought of in terms of a "yield stress" for whatever combined mechanisms may occur and this will be briefly considered further in Section 3.

Finally, the possible effects of elastic anisotropy, elastic recovery or the local relaxation of the five independent slip system criterion around hardness indentations in solids of high E/Y ratio have been too complex for further investigation but may play some role in the indentation process.

3. The yield stress

Johnson [35] and Studman *et al.* [36] have developed the "spherical cavity model" of the indentation process, originally devised for brittle solids by Marsh [9], whereby displaced material is accommodated by elastic compression and the displacements are radial rather than directed towards the surface to form a "pile-up". One consequence of the "radial displacement model" is that it enables an equation to be derived relating hardness to the plastic yield stress [35, 37, 38]:

$$\frac{H}{Y} = \frac{1}{2} + \frac{2}{3}\left[1 + \ln\left\{\frac{(E/Y)\tan\beta + 4(1-2\nu)}{6(1-\nu)}\right\}\right], \quad (1)$$

where ν is Poisson's ratio and β the contact angle between the indenter facet and the surface of the solid under test.

In situations where this model is thought to apply, the plastic yield stress (Y) can be calculated by an iterative method [37]. Unfortunately, measured hardness values depend strongly on the load used, and the model does not allow for this indentation size effect [25]. Nevertheless, taking $E = 469$ GPa and $\nu = 0.17$ [27, 39, 40], and using the hardness pressures quoted in the previous section, the plastic yield stress is calculated to be between 12 and 52 GPa (i.e. $G/17$ and $G/4$ taking $G = 193$ GPa [28]). This upper limit is in the same range as the theoretical shear strength calculated previously (allowing for the very rough nature of such estimates) but does not allow any conclusions to be drawn as to the deformation mechanisms involved, i.e. distinguishing dislocation slip from block shear, slip or densification.

4. Modelling hardness anisotropy – the ERSS model

The ERSS model of Brookes *et al.* has successfully explained observed hardness anisotropies* on a range of single-crystal materials and has only failed where twinning [2] or indentation creep has had an effect [41]. This success is surprising as the model is only concerned with the geometry of discrete slip systems and does not consider the differing Peierls' stresses and mobilities of dislocations of different character on identical slip systems (e.g. [4, 42]) or other aspects of both yielding and work hardening. It also makes an assumption about the stress state (i.e. that it is predominantly tensile in the critical region controlling the plastic behaviour) which is believed by some workers to be untrue (e.g. [26]). For

*It should be appreciated that the mm2 plane symmetry of the Knoop indenter limits the experimentally observed hardness anisotropy to belonging to the Laue class of the crystal. Thus details of point group or space group control of deformation mechanisms (e.g. the effect of polarity of SiC crystals) cannot be established in this way.

example, for low E/Y materials, where most of the deformation occurs immediately beneath the indenter [13], a compressive model based on the radial forces would appear to be more appropriate. However, Brookes *et al.* found that a model based on tensile rather than compressive forces generally agreed with the experimental data [1] although Armstrong and co-workers have used a compressive force version to examine work-hardening effects [43, 44].

The Brookes' model essentially considers an effective resolved shear stress (ERSS) which is the Schmidt–Boas resolved shear stress, τ, corrected by a *constraint factor* (CF – see next section) which was introduced in an attempt to allow for the constraints on plastic flow imposed by the presence of both the indenter and the elastic hinterland [1], i.e.

$$\tau = (L/A) \cos \lambda \cos \phi \qquad (2)$$

$$\text{ERSS} = \tau \times 0.5[\sin \gamma + \cos \psi] \qquad (3)$$

where L is the force on a cylindrical test element of cross-sectional area A, and thus the function F is defined for the ith facet of the indenter by

$$\text{ERSS} = (L/A)\, F(\lambda, \phi, \gamma, \psi) \qquad (4)$$

where the symbols and angles are defined in Fig. 7 of [1]. Furthermore, the present study has used a method developed and discussed by Arnell [2] whereby the hardness (H) is related to the critical resolved shear stress (CRSS) for yield by a geometrical factor f, i.e.

$$H \propto (\text{CRSS})\, f \qquad (5)$$

where f is the function $1/F$ summed over all facets. f is then calculated for each slip system, for each crystal section and for every indenter orientation on that section.* However, while this method predicts the shape of the anisotropy it gives no indication of its magnitude (e.g. the observed 5 : 1 difference in magnitude for the same anisotropy observed in isostructural MgO and LiF).

The further effect of work hardening has not been satisfactorily incorporated into any model and it has been argued that it can either increase or decrease the magnitude of the anisotropy, namely:

(a) that the work-hardening term is itself strongly anisotropic and thus increases the magnitude of the hardness anisotropy from that given by the geometrical formula alone [43].

(b) that the work hardening term is fairly isotropic and thus decreases the relative magnitude of the calculated anisotropy [2].

Therefore, in order to elucidate the effects of work hardening or hardness anisotropy, it is at least necessary to consider possible dislocation reactions in detail. This has not been considered further here, but an example of a possible work-hardening effect is described in Section 7.

5. Modelling hardness anisotropy – the constraint factor

The suggestion that the geometry of the indenter itself might provide a constraint on the displacement experienced by slipped material was first made by Daniels and Dunn [45] who added a factor $\cos(\psi)$ to the Schmidt–Boas formula (Equation 2) to allow for slip plane rotation, this being easiest when the axis of rotation of the slip system lies in the plane of the indenter facet. However, this model could not account for the various $\{1\,1\,0\}$ slip plane activities observed by Brookes *et al.* in MgO [1] and they suggested a more complex constraint involving the angular orientations (γ and ψ) of both the axis of rotation and the slip direction to the facet horizontal. This led them to decide upon the following boundary conditions:

$$\text{CF} = 0 \text{ when } \gamma = 0 \text{ (which makes } \psi = 90),$$

i.e. the constraint is a maximum when the slip direction is parallel to the facet (and thus the rotation axis is perpendicular to the horizontal line in the indenter facet).

$$\text{CF} = 1 \text{ when } \psi = 0 \text{ (which makes } \gamma = 90),$$

i.e. the constraint is a minimum when the rotation axis is parallel to the facet (and thus the slip direction is not parallel to the facet, so material can flow upwards [1]).

The function used by Brookes *et al.* is one of the simplest to fulfil these conditions, namely:

$$\text{CF} = 0.5[\cos \psi + \sin \gamma]. \qquad (6)$$

It should be emphasised that this constraint factor appears to be inappropriate for stiff, brittle ceramics which are thought to conform to indentation by radial displacements and have been

*A listing of the program in FORTRAN is available on application to the authors.

observed not to form surface "pile-ups". However, in the absence of a more appropriate formulation of the likely constraints in these cases, and, since the ERSS model with Brookes' constraint seems to have successfully described the hardness anisotropy observed in a large number of ceramics, these boundary conditions have been retained here. There is obvious scope for extending this study by considering boundary conditions which (a) take account of radial displacements and (b) include a third angle because two angles alone do not uniquely define the orientation of the slip system with respect to the indenter.

Further constraints regarding the direction of material flow, either upward or radially, depend critically on the ductile/elastic character of the material in terms of its E/Y ratio. Thus, if the controlling slip systems could be identified independently, the precise form of the observed hardness anisotropy might be used to investigate differences in the relative importance of radial and surface-directed displacements by adjusting the constraint factor until the model fitted the results. However, such an approach has not been followed further here.

It is unlikely that there would be discontinuities in the gradient of the function CF with respect to the angles ψ and γ. So additional conditions would be:

$$\left.\frac{\partial CF}{\partial \alpha}\right|_{\alpha-} = \left.\frac{\partial CF}{\partial \alpha}\right|_{\alpha+} \quad (7)$$

where α is any and all of the angles λ, ϕ, γ and ψ. This means that any function that can be expressed as a Fourier series could be a suitable constraint function.

However, if a variety of constraint functions are used to calculate effective resolved shear stress plots, the variations between them will give some idea of the confidence which can be placed in them. For slip systems and indentation planes where the predictions are in good agreement, deviations of the experimental anisotropy from these predictions would strongly suggest either that another deformation mode was important (e.g. another slip system, twinning, or densification) or that the work hardening could be strongly orientation dependent in that particular material. If, for some slip systems and some crystal sections, there are large variations in anisotropy when using different constraint factors, then little reliance should be placed on the model in these cases.

To test the stability of the model with respect to variations in the form of the constraint factor, three functions were chosen in addition to that of Brookes *et al.*, namely:

$$CF(2) = 0.5[(\cos\psi)^{1/4} + (\sin\gamma)^{1/4}] \quad (8)$$

$$CF(3) = 0.5[(\cos\psi)^{4} + (\sin\gamma)^{4}] \quad (9)$$

$$CF(4) = 0.5[(\cos\psi)^{4} + (\sin\gamma)^{1/4}]. \quad (10)$$

CF(2) is much 'steeper', and CF(3) more gently sloping than that of Equation 6 at low and high values of ψ and γ, but the reverse is the case in the middle range. CF(4) is asymmetric with respect to $\gamma = 90 - \psi$. These specific functions were chosen because they encompass a reasonable range of values (see Fig. 1) apparently wide enough to clearly display the stability of the ERSS model for basal and prismatic slip as compared with the instability for pyramidal slip (see section 7). In Figs. 3 to 5, the expected forms of the hardness anisotropies for each of the constraint factors have been superposed and this means that there is now an intrinsic measure of the reliability of the ERSS model. When the model is unstable with respect to small changes model is unstable with respect to small changes in the constraint factor, it should be used with caution; up till now it has not been possible to distinguish these situations from those where the model is well behaved.

It has already been shown that the yield stress of SiC can be determined and now the ERSS model will be used to distinguish between glide of different slip systems.

6. Experimental determination of hardness anisotropy

Silicon carbide single crystals were separated from blue–black Acheson aggregates supplied by Arendal Smeltewerk (Norway). The crystals were generally platelets with extensive (~ 10 mm square) basal surfaces bounded by a number of prominent cleavage or growth facets and were up to 3 mm thick. The orientation of the crystal axes in these platelets was established by means of back-reflection Laue photographs taken with the X-ray beam perpendicular to the basal surface. The principal zones in these photographs were recognized from a standard [0 0 0 1] Laue photograph, itself indexed by comparison with an electron diffraction pattern of the same specimen, using a cleavage facet as a reference. By comparison with published Laue photographs [46], the crystals appeared to contain mixed stacking

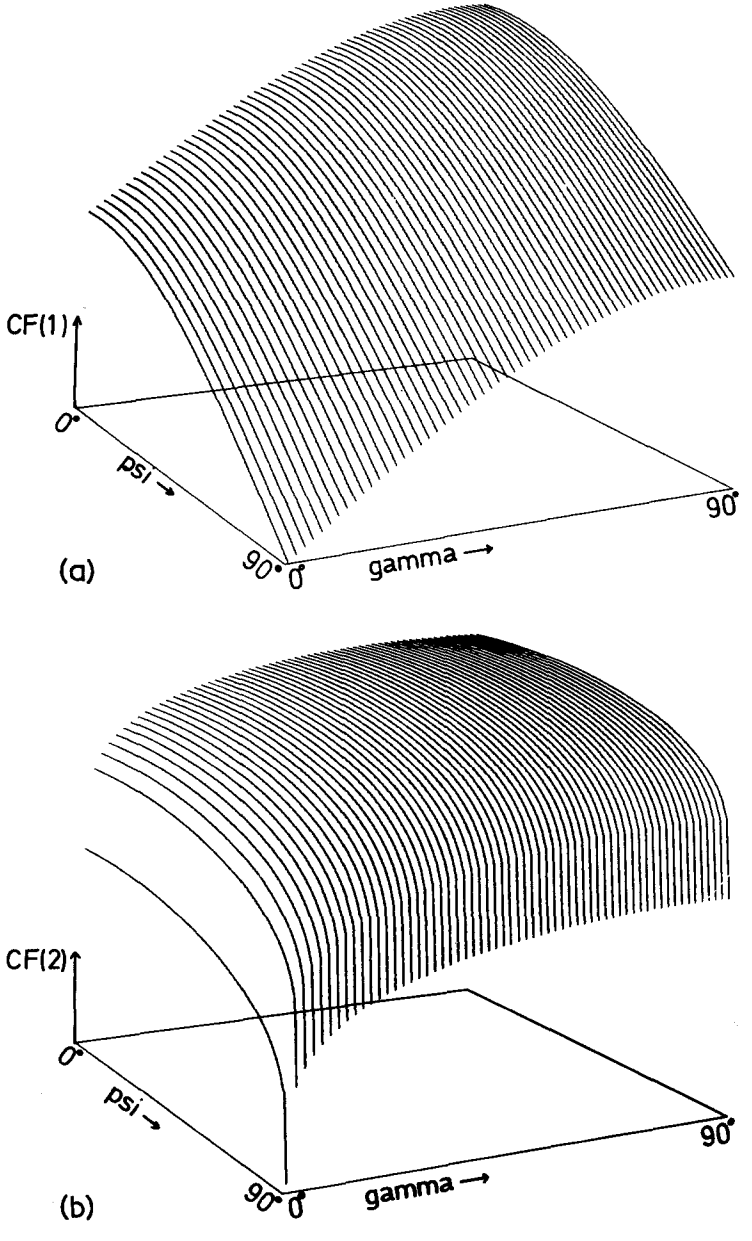

Figure 1 Three-dimensional plots of the four constraint factors: (a) equation 6, (b) equation 8, (c) equation 9, and (d) equation 10.

sequences presumed to be predominantly of the 6H [47] polytype and all crystallographic indexing has been based on this assumption (see also the concluding remarks of Section 7). Specimens for basal plane tests were obtained by mounting and polishing the as-grown basal surfaces, whilst $\{1\,\bar{1}\,0\,0\}$ and $\{1\,1\,\bar{2}\,0\}$ sections were obtained by cutting a crystal of previously determined orientation using a Capco Q35 annular diamond saw, the orientation of the cut surface being confirmed by a second Laue photograph. All specimens were mounted in resin and polished with diamond paste to a 0.25 μm finish prior to hardness testing [47].

Microhardness indentations were made and measured under ambient laboratory conditions using a Leitz Miniload which had been fitted with a rotating stage and angular scale. Although it is difficult to make meaningful comparisons of the absolute values obtained in separate microhardness experiments, it is possible to obtain reproducible self-consistent trends (e.g. in anisotropy) in a given experiment, provided certain precautions are taken. Therefore care was taken to ensure that the specimen was aligned correctly such that the indentations were symmetrical. The limit of acceptability was taken as an asymmetry of 10%

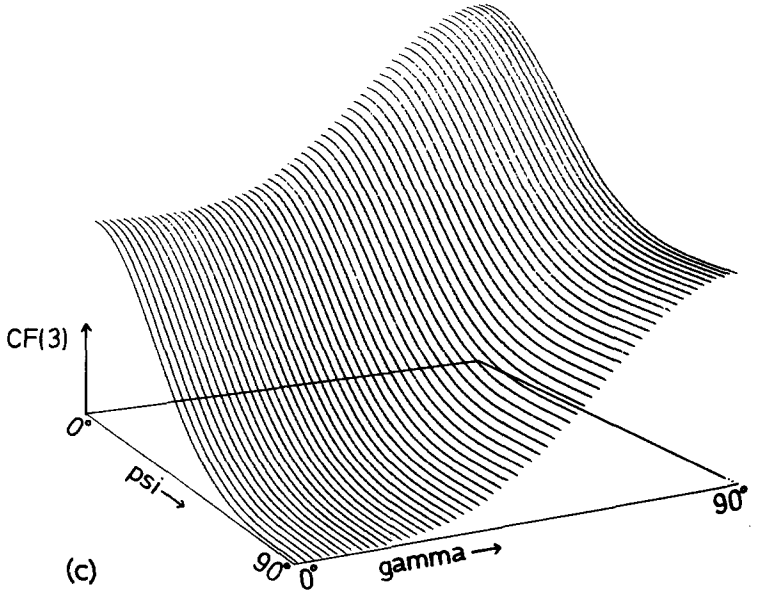

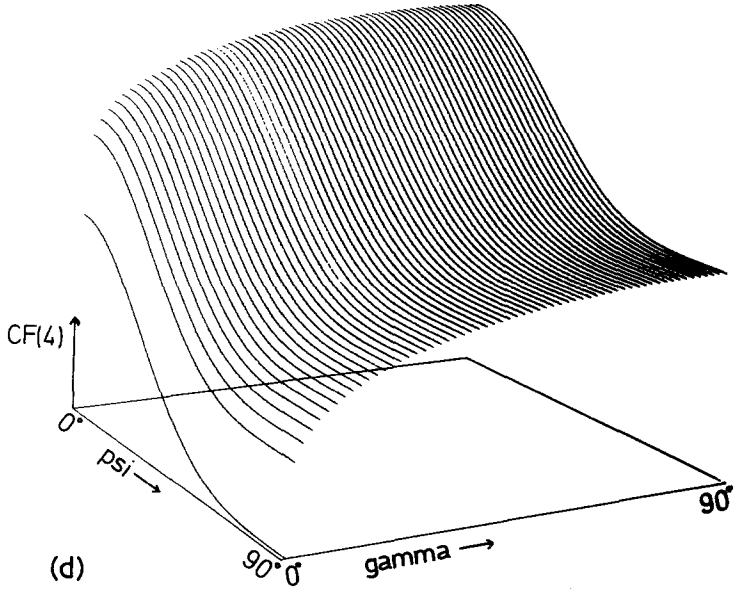

which has been shown by Thibault and Nyquist [48] to produce no measurable change in the size of the indentation. A standard loading cycle, using a rise time of 12 sec followed by 18 sec at full load, was used for all tests to eliminate variations due to indentation creep. All measurements used to generate one anisotropy curve were made using the same specimen and indenter and the indentations were made in a single session to eliminate variations due to changes in the environment or specimen setting, etc. The indentations were measured by a single observer in a single session, not necessarily at the same time as they were made, under consistent lighting conditions (artificial lighting in a darkened room). This eliminated any inconsistencies due to changes in visual performance of the observer.

For loads of 300 gf (2.94 N) and 500 gf (4.9 N), the Knoop hardness as a function of crystallographic orientation on the basal plane was determined from the average lengths of sets of ten indentations for each indenter orientation, measurements being made at 10° intervals over a 60° range, starting with the long axis of the indenter parallel to the trace of a $\{1\,\bar{1}\,0\,0\}$ facet (i.e. along $\langle 1\,1\,\bar{2}\,0\rangle$). These two loads were chosen because Knoop

indentations made with a load of 300 gf did not show a significant amount of indentation fracture whilst those made with a load of 500 gf did. It was found that the microhardness anisotropy was similar in both cases and thus not significantly affected by the incidence of cracking. This observation can be justified by considering the proportion of work done by the indenter which is used to create the fracture surfaces, typically less than 0.1% [49]. Measurements of Knoop microhardness anisotropy on $\{1\,\bar{1}\,0\,0\}$ and $\{1\,1\,\bar{2}\,0\}$ were performed with a 500 gf load only. On these prism planes measurements were made at 10° intervals over a 90° range starting with the long axis of the indenter parallel to the trace of $\{0\,0\,0\,1\}$, again taking the arithmetic mean over ten indentations at each orientation.

7. Results and discussion

Typical hardness anisotropy data for each of the principal sections are presented graphically in Fig. 2. For each of these planes, simulations were obtained of the angular variation of the geometrical factor f, for a number of families of slip systems identified in SiC such as $\{0\,0\,0\,1\}\langle 1\,1\,\bar{2}\,0\rangle$, $\{1\,\bar{1}\,0\,0\}\langle 1\,1\,\bar{2}\,0\rangle$ [10] and various systems of the type $\{h\,\bar{h}\,0\,l\}\langle 1\,1\,\bar{2}\,0\rangle$ as well as other conceivable candidates, such as $\{1\,1\,\bar{2}\,0\}\langle 1\,\bar{1}\,0\,0\rangle$. A selection of curves of f as a function of indenter orientation are shown in Figs. 3–5.

The hardness anisotropy of the basal plane (Fig. 2a) is modelled most successfully by assuming $\{1\,\bar{1}\,0\,0\}\langle 1\,1\,\bar{2}\,0\rangle$ slip (Fig. 3b), corroborating the findings of Adewoye and Page [13], even the cusp around $[1\,0\,\bar{1}\,0]$ being reproduced. The shaded bands in Fig. 3 show the spread of results obtained by using the four constraint factors. It can be seen that using only the constraint factor of Brookes *et al.*, the slip system $\{1\,\bar{1}\,0\,1\}\langle 1\,1\,\bar{2}\,0\rangle$ might also be considered a likely candidate, but for such pyramidal slip systems the ERSS model is unreliable because of its sensitivity to the precise form of the constraint function (cf. Fig. 3b and d and note the different vertical scales).

The hardness anisotropy on the prism planes (Fig. 2b and c) is considerably more marked than that observed on the basal plane. In each case the lowest hardness was found with the long axis of the indenter parallel to $[0\,0\,0\,1]$ (in accordance with the data of Shaffer). This was interpreted by Brookes *et al.* as indicative of $\{1\,\bar{1}\,0\,0\}\langle 1\,1\,\bar{2}\,0\rangle$ slip which, taking these limits in isolation, is consistent with the simulations of their model. However, the present work shows that the measured hardness value does not vary monotonically between the two principal orientations. Instead

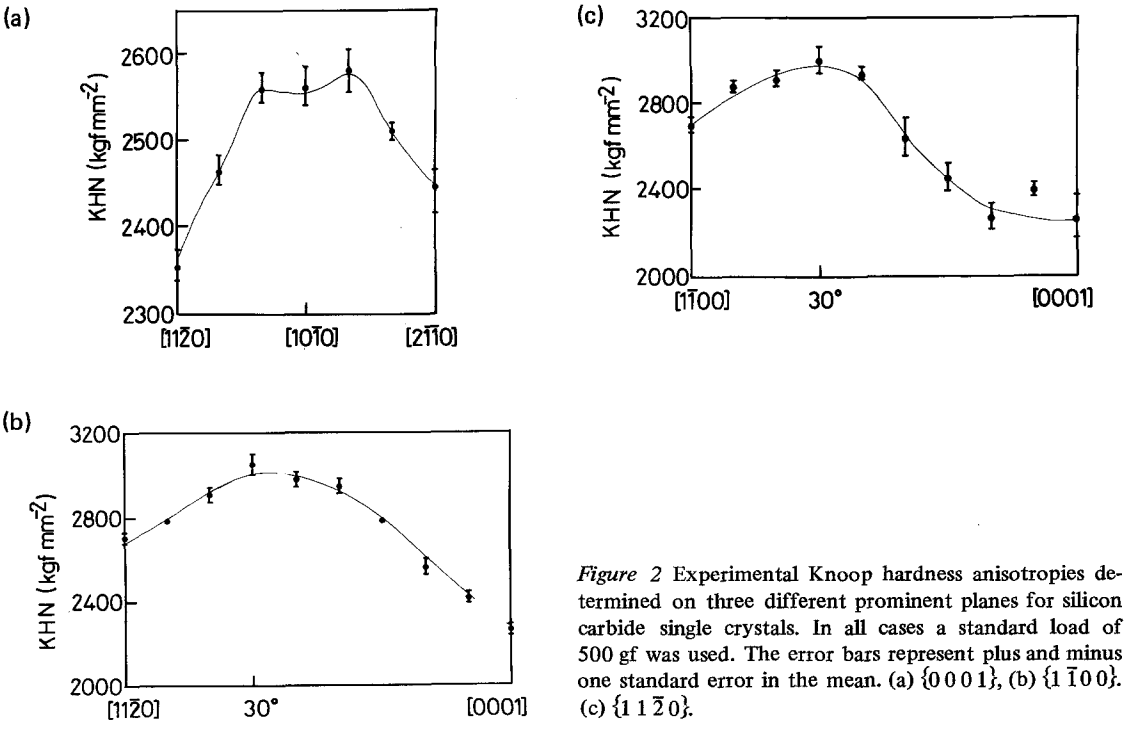

Figure 2 Experimental Knoop hardness anisotropies determined on three different prominent planes for silicon carbide single crystals. In all cases a standard load of 500 gf was used. The error bars represent plus and minus one standard error in the mean. (a) $\{0\,0\,0\,1\}$, (b) $\{1\,\bar{1}\,0\,0\}$. (c) $\{1\,1\,\bar{2}\,0\}$.

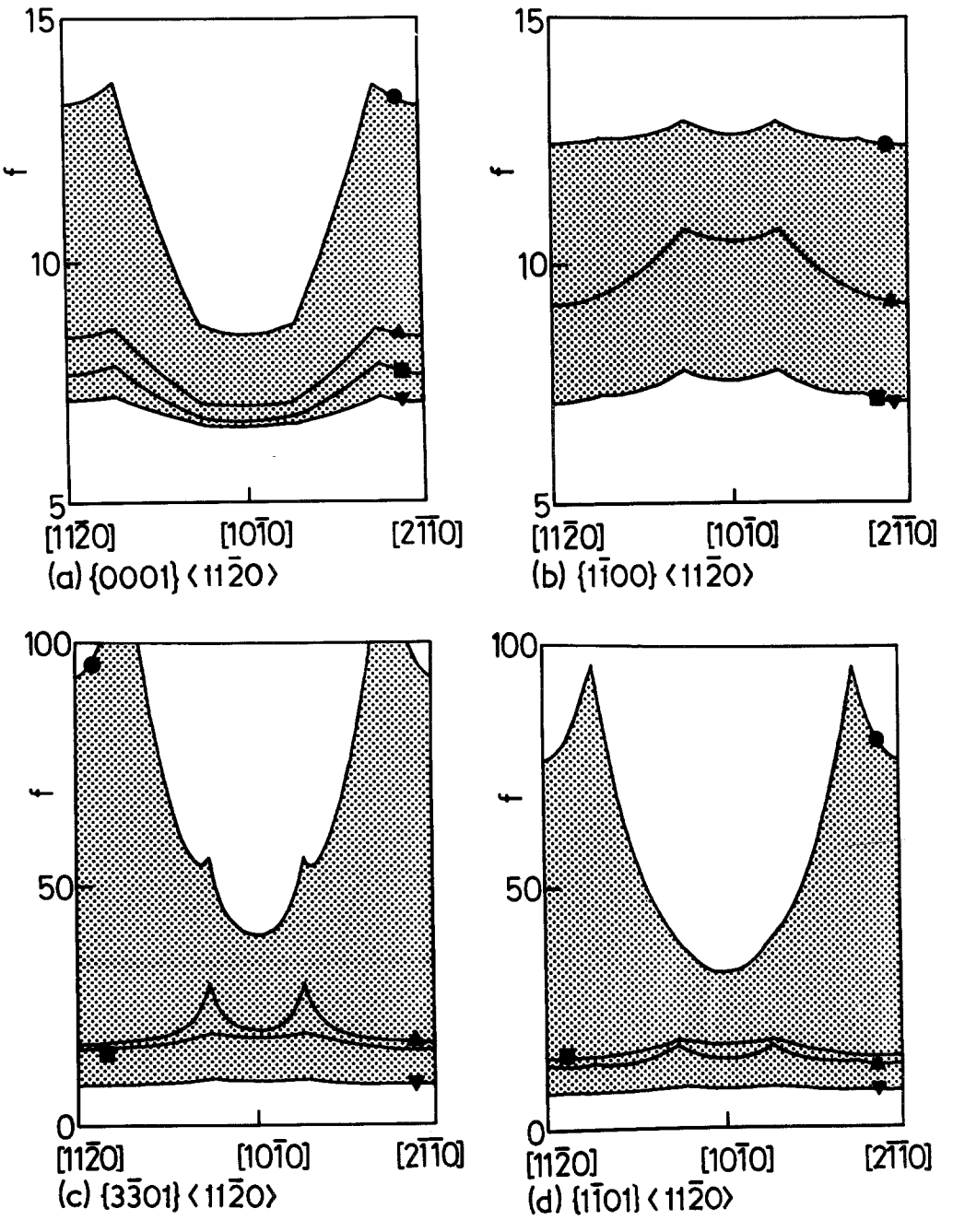

Figure 3 f plot on the (0 0 0 1) section for four different slip systems: (a) {0 0 0 1}⟨1 1 $\bar{2}$ 0⟩, (b) {1 $\bar{1}$ 0 0}⟨1 1 $\bar{2}$ 0⟩, (c) {3 $\bar{3}$ 0 1}⟨1 1 $\bar{2}$ 0⟩, (d) {1 $\bar{1}$ 0 1}⟨1 1 $\bar{2}$ 0⟩. In this figure, together with Figs. 4 and 5 the line calculated using CF(1) is labelled with ▲; using CF(2), with ▼; using CF(3), with •; and using CF(4), with ■. Note the different scales on the *f* axes.

there is an intermediate peak hardness at approximately 60° from [0 0 0 1] in each case and the observed hardness anisotropy does not correspond to the simulation of that due to any of the likely slip systems acting in isolation. However, it is possible to interpret the observed anisotropy on {1 $\bar{1}$ 0 0} and {1 1 $\bar{2}$ 0} in terms of the joint action of the two most probable slip systems; {1 $\bar{1}$ 0 0} ⟨1 1 $\bar{2}$ 0⟩ and {0 0 0 1}⟨1 1 $\bar{2}$ 0⟩. Taking {1 $\bar{1}$ 0 0} for example, Fig. 4a and b show that, when the indenter axis is parallel to [0 0 0 1], the expected *f* value for {1 $\bar{1}$ 0 0}⟨1 1 $\bar{2}$ 0⟩ slip is low, whilst that for {0 0 0 1}⟨1 1 $\bar{2}$ 0⟩ is slightly higher and would create an (unobserved) hardness peak 10°

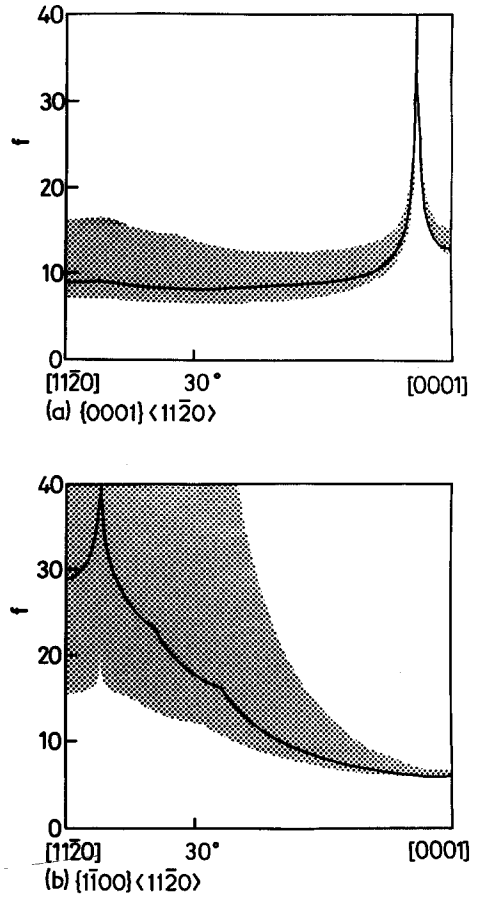

Figure 4 f plot on the $(1\,\bar{1}\,0\,0)$ section for the two slip systems: (a) $\{0\,0\,0\,1\}\langle 1\,1\,\bar{2}\,0\rangle$, (b) $\{1\,\bar{1}\,0\,0\}\langle 1\,1\,\bar{2}\,0\rangle$. (See Fig. 3 for key to symbols.)

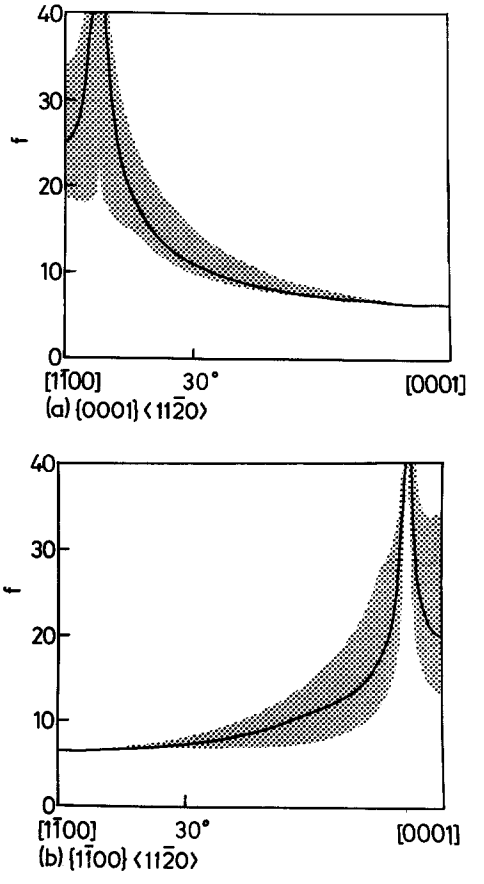

Figure 5 f plot on the $(1\,1\,\bar{2}\,0)$ section for two slip systems: (a) $\{0\,0\,0\,1\}\langle 1\,1\,\bar{2}\,0\rangle$, and (b) $\{1\,\bar{1}\,0\,0\}\langle 1\,1\,\bar{2}\,0\rangle$. (See Fig. 3 for key to symbols.)

from $[0\,0\,0\,1]$. Thus the former appears to be the preferred slip system at this indenter orientation implying that, since the f values for the two systems are nearly equal, the CRSS for $\{1\,\bar{1}\,0\,0\}$ slip is less than that for $\{0\,0\,0\,1\}$ slip (and this is confirmed below). However, if this slip system alone were controlling the hardness, it would cause an increase in hardness to a maximum with the indenter 80° from $[0\,0\,0\,1]$. Thus the decrease in hardness between 60° and 90° from $[0\,0\,0\,1]$ must be due to activation of another slip system. Now, comparison of Fig. 4a and b shows that, for indenter orientations near $[1\,1\,\bar{2}\,0]$, the $\{0\,0\,0\,1\}\langle 1\,1\,\bar{2}\,0\rangle$ slip system experiences a considerably higher effective resolved shear stress (i.e. a much lower f factor) than $\{1\,\bar{1}\,0\,0\}\langle 1\,1\,\bar{2}\,0\rangle$, which should be enough to counteract its presumed higher critical resolved shear stress and produce slip on that system. Thus the controlling slip system may change from $\{1\,\bar{1}\,0\,0\}\langle 1\,1\,\bar{2}\,0\rangle$ to $\{0\,0\,0\,1\}\langle 1\,1\,\bar{2}\,0\rangle$ as the indenter is rotated. In order to correspond with the experimentally observed intermediate hardness peak (Fig. 2b), the change-over must occur when the indenter is aligned with its long axis at approximately 60° from $[0\,0\,0\,1]$. If the curves are superposed and offset to cross at this orientation (Fig. 6), a curve of f is obtained which increases steadily from $[0\,0\,0\,1]$ through 60° of rotation and then is almost flat onto $[1\,1\,\bar{2}\,0]$. A similar effect can be argued for the observed behaviour on $\{1\,1\,\bar{2}\,0\}$.

At the change-over point the expected hardness due to both slip systems must be the same, and, from Equation 6, it can be seen that if the ratio of f values at this point is known, then the ratio of the critical resolved shear stresses is equal to its inverse.

If it is accepted that there is a good likelihood of the "real" constraint being represented by a function in the range of those four functions described previously, then a range of f values for

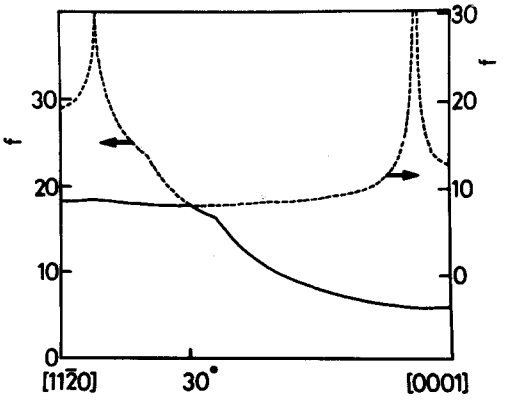

Figure 6 Superposition of f plots from Fig. 5a and b showing how the operation of two slip systems over different angular ranges ray be combined to explain the experimental data of Fig. 2b.

each slip system is obtained at the change-over point. Thus, by considering the crossover on $\{1\,\bar{1}\,0\,0\}$, the ratio CRSS $\{0\,0\,0\,1\}\langle 1\,1\,\bar{2}\,0\rangle$: CRSS $\{1\,\bar{1}\,0\,0\}\langle 1\,1\,\bar{2}\,0\rangle$ must lie between 0.88 and 4.69. Similarly, by considering the crossover on $\{1\,1\,\bar{2}\,0\}$, this ratio can be narrowed to lie between 1.18 and 2.10.

This simple superposition does not correspond precisely to the experimental hardness data, but as yet no account has been taken of work hardening when there are two operating slip systems. With the indenter axis parallel to $[0\,0\,0\,1]$, $\langle 1\,1\,\bar{2}\,0\rangle$, or $\langle 1\,\bar{1}\,0\,0\rangle$ only one slip system is dominantly active, but, in the angular range around the crossover, work-hardening effects due to multiple slip could cause the observed hardness peak. Although there are no locking reactions that can occur between any members of the two slip system families, new glissile dislocations formed by such relations as

$$\frac{a}{3}[1\,1\,\bar{2}\,0]_{(0001)} + \frac{a}{3}[\bar{2}\,1\,1\,0]_{(01\bar{1}0)} \rightarrow \frac{a}{3}[\bar{1}\,2\,\bar{1}\,0]_{(0001),(10\bar{1}0)} \qquad (11)$$

are likely, because of their geometry, to experience an effective resolved shear stress less than that on either of the primary systems. This would produce the required apparent work-hardening effect.

The two slip systems $\{0\,0\,0\,1\}\langle 1\,1\,\bar{2}\,0\rangle$ and $\{1\,\bar{1}\,0\,0\}\langle 1\,1\,\bar{2}\,0\rangle$ have only four independent shear strains between them. However, possible densification, microcracking and elastic compression probably removes the necessity to conform to the five-shear strains criterion and thus no slip on pyramidal slip systems, such as $(h\,\bar{h}\,0\,l\}\langle 1\,1\,\bar{2}\,0\rangle$, seems to be required, although some may occur. Further, since the two observed slip systems generate the same hardness anisotropies in all alpha structure polytypes [50], the deduced behaviour is independent of the polytypic state of the crystals used in the experiments.

While other combinations of slip systems might produce anisotropies similar to those observed, the explanation suggested here seems the simplest consistent with the experimental data and likely slip geometries in silicon carbide.

8. Conclusions

It has been shown that despite the complex nature of the deformation process beneath a sharp indenter, particularly in the early stages of indentation when very large non-equilibrium stresses prevail, it is reasonable to interpret the experimentally observed *anisotropy* in Knoop microhardness in terms of dislocation slip using a model of the effective resolved shear stress type. Further, the degree of confidence to be placed in the correlation of the model's predictions with experimental data has been assessed by varying the range of the constraint factor within Brookes *et al.*'s boundary conditions.

Using the radial displacement model of indentation deformation, the room temperature yield stress of silicon carbide has been deduced to lie in the range 12 to 52 GPa.

It has been shown that the observed hardness anisotropy on $\{0\,0\,0\,1\}$ planes is consistent with that predicted for the $\{1\,\bar{1}\,0\,0\}\langle 1\,1\,\bar{2}\,0\rangle$ slip system and that, although some slip systems of the type $\{h\,\bar{h}\,0\,l\}\langle 1\,1\,\bar{2}\,0\rangle$ would give the same general anisotropy, less confidence could be placed in these predictions since different constraint factors gave widely varying results (cf. Fig. 3c and d). However, the observed anisotropy on prism planes was found to be incompatible with that predicted for $\{1\,\bar{1}\,0\,0\}\langle 1\,1\,\bar{2}\,0\rangle$ alone, and, in this case, the joint action of $\{1\,\bar{1}\,0\,0\}\langle 1\,1\,\bar{2}\,0\rangle$ and $\{0\,0\,0\,1\}\langle 1\,1\,\bar{2}\,0\rangle$ was required to match the experimental data. Each slip system was found to be preferred over a certain range of orientation with a transition at about 60° away from $[0\,0\,0\,1]$. The ratio of CRSS for $\{0\,0\,0\,1\}\langle 1\,1\,\bar{2}\,0\rangle$ slip to that for $\{1\,\bar{1}\,0\,0\}\langle 1\,1\,\bar{2}\,0\rangle$ was deduced to be in the range 1.2 to 2.1.

Thus the evidence indicates that plastic deformation under hardness indentations in SiC at room temperature may occur preferentially on the

$\{1\bar{1}00\}\langle 11\bar{2}0\rangle$ slip system, but may also occur on the $\{0001\}\langle 11\bar{2}0\rangle$ system for certain orientations of the indenter.

Acknowledgements

The authors are indebted to Professor R. W. K. Honeycombe for laboratory facilities, the University of Cambridge Computing Service for the use of computing and plotting facilities, the SRC for a maintenance grant for one of us (PMS) and the European Research Office of the US Army for financial support (GRS) during the period when this work was performed.

References

1. C. A. BROOKES, J. B. O'NEILL and B. A. W. REDFERN, *Proc. Roy. Soc. London* **A322** (1971) 73.
2. R. D. ARNELL, *J. Phys. D.* **7** (1974) 1225.
3. G. MORGAN and M. H. LEWIS, *J. Mater. Sci.* **9** (1974) 349.
4. B. J. HOCKEY, "The Science of Hardness Testing and its Research Applications" (American Society for Metals, Metals Park, Ohio, 1973) p. 21.
5. Y. HUMASHIRO, A. ITOH, T. KINOSHITA and M. SOBAJINA, *J. Mater. Sci.* **12** (1977) 595.
6. D. J. ROWCLIFFE and G. E. HOLLOX, *ibid* **6** (1971) 1261.
7. *Idem, ibid* **6** (1971) 1270.
8. R. H. J. HANNINK, D. L. KOHLSTEDT and M. J. MURRAY, *Proc. Roy. Soc. London* **A326** (1972) 409.
9. D. M. MARSH, *ibid* **A279** (1964) 420.
10. O. O. ADEWOYE, Ph.D. Thesis, University of Cambridge (1976).
11. G. R. SAWYER, Ph.D. Thesis, University of Cambridge (1979) in preparation.
12. A. W. RUFF and S. M. WIEDERHORN, in "Materials Erosion", Treatise on Materials Science and Technology, Vol. 16, edited by C. M. Preece (Academic Press, New York, 1979) ch. 2.
13. O. O. ADEWOYE and T. F. PAGE, *J. Mater. Sci.* **11** (1976) 981.
14. T. F. PAGE, G. R. SAWYER, O. O. ADEWOYE and J. J. WERT, *Proc. Brit. Ceram. Soc.* **26** (1978) 193.
15. P. T. B. SHAFFER, *J. Amer. Ceram. Soc.* **47** (1964) 466.
16. P. HAASON, *J. de Physique: Dissociation des Dislocations, Beaune, Colloque* **7** (1974) 167.
17. V. I. ZAITSEV, V. I. BARBASHOV and Yu. B. TKACHENKO, *Phys. Stat. Sol.* **A44** (1977) K39.
18. B. R. LAWN and R. WILSHAW, *J. Mater. Sci.* **10** (1975) 1049.
19. J. J. GILMAN, "The Science of Hardness Testing and its Research Applications" (American Society for Metals, Metals Park, Ohio, 1973) p. 54.
20. I. V. GRIDNEVA, Yu. V. MILMAN and V. I. TREFILOV, *Phys. Stat. Sol.* **A14** (1972) 177.
21. J. A. VAN VECHTEN, *Phys. Rev.* **B7** (1973) 1479.
22. V. I. TREFILOV, V. A. BORISENKO, G. G. GNESIN, I. V. GRIDNEVA and Yu. V. MILMAN, *Dokl. Akad. Nauk. SSSR* **239** (1977) 579 (in Russian).
23. M. A. VELEDNITSKAYA, V. N. ROZHANSKII, L. F. COMOLOVA, G. V. SAPARIN, J. SCHREIBER and O. BRUMMER, *Phys. Stat. Sol.* **A32** (1975) 123.
24. V. N. ROZHANSKII, M. P. NAZAROVA, I. L. SVETLOV and L. K. KALASHNIKOVA, *ibid* **41** (1970) 579.
25. P. M. SARGENT and T. F. PAGE, *Proc. Brit. Ceram. Soc.* **26** (1978) 209.
26. D. TABOR, *Rev. Phys. Technol.* **1** (1970) 145.
27. J. W. EDINGTON, D. J. ROWCLIFFE and J. L. HENSHALL, *Powder Met. Int.* **7** (1975) 82.
28. R. C. MARSHALL, J. W. FAUST and C. E. RYAN (ed.), "Silicon Carbide 1973", Proceedings of the Conference, Miami Beach (University of South Carolina Press, Columbia, South Carolina, 1974).
29. B. J. HOCKEY and B. R. LAWN, *J. Mater. Sci.* **10** (1975) 1275.
30. B. J. HOCKEY, S. M. WIEDERHORN and H. JOHNSON, in "Fracture Mechanics of Ceramics", Vol. 3, edited by R. C. Bradt, D. P. H. Hasselmann and F. F. Lange (Plenum, New York, 1978) p. 379.
31. R. W. ARMSTRONG and C. Cu. WU, *J. Amer. Ceram. Soc.* **61** (1978) 102.
32. E. B. LEIKO, A. LUFT and E. M. NADGORNII, *Phys. Stat. Sol.* **A44** (1977) 285.
33. T. F. PAGE and J. J. WERT, unpublished work.
34. R. P. BURNAND, Ph.D. Thesis, University of Exeter (1972).
35. K. L. JOHNSON, *J. Mech. Phys. Sol.* **18** (1970) 115.
36. C. J. STUDMAN, M. A. MOORE and S. E. JONES, *J. Phys. D.* **10** (1977) 949.
37. M. A. MOORE, Ph.D. Thesis, University of Newcastle (1974).
38. C. J. STUDMAN and J. E. FIELD, *J. Phys. D.* **9** (1976) 857.
39. R. D. CARNAHAN, *J. Amer. Ceram. Soc.* **51** (1968) 223.
40. P. T. B. SHAFFER and C. K. JIN, *Mat. Res. Bull.* **7** (1972) 63.
41. C. A. BROOKES, R. P. BURNAND and J. E. MORGAN, *J. Mater. Sci.* **10** (1975) 2171.
42. Yu. S. BOYARSKAYA and D. Z. GRABKO, *Kristall und Technik* **8** (1973) 1367.
43. R. W. CALDER and R. W. ARMSTRONG, *Mater. Sci. Eng.* **12** (1973) 59.
44. R. W. ARMSTRONG and A. C. RAGHURAM, "The Science of Hardness Testing and irs Research Applications" (American Society for Metals, Metals Park, Ohio, 1973) p. 175.
45. F. W. DANIELS and C. G. DUNN, *Trans. Amer. Soc. Metals* **41** (1949) 419.
46. Y. TUNG and J. W. FAUST Jr, in "Silicon Carbide 1973", Proceedings of the Conference, Miami Beach (University of South Carolina Press, Columbia, South Carolina, 1974) p. 246.
47. G. R. SAWYER and T. F. PAGE, *J. Mater. Sci.* **13** (1978) 865.

48. N. W. THIBALT and H. L. NYQUIST, *Trans. Amer. Soc. Metals* **38** (1947) 271.
49. P. M. SARGENT and G. R. SAWYER, unpublished work.
50. P. M. SARGENT, unpublished work.

Received 31 May and accepted 29 August 1979.